論文 / 著書情報
Article / Book Information

論題(和文)	Physics-Informed Wind Force Prediction and Structural Validation Part1: Physics-Informed Prediction of Wind Force Time Histories
Title(English)	
著者(和文)	LONG YIZHOU, 佐藤大樹, 陳引力, 田中英之
Authors(English)	Long Yizhou, Daiki Sato, Yinli Chen, Hideyuki Tanaka
出典 / Citation	日本建築学会関東支部研究報告集， I， ，pp. 541-544
Citation(English)	， I， ，pp. 541-544
発行日 / Pub. date	2026，3
権利情報	一般社団法人 日本建築学会

2025年度日本建築学会
関東支部研究報告集 I
2026年3月

Physics-Informed Wind Force Prediction and Structural Validation Part 1: Physics-Informed Prediction of Wind Force Time Histories

構造-振動

正会員 ○ LONG YIZHOU[*1] 同 佐藤 大樹[*2]
陳 引力[*3] 田中 英之[*4]

Physics-Informed Neural Networks (PINN), Wind Load Prediction, Deep Learning, Power Spectral Density (PSD), Inter-Story Coherence, Wind Tunnel Validation

1 INTRODUCTION

Wind-induced vibrations present a critical design issue for tall and base-isolated buildings, whose elongated fundamental periods often lead to wind-governed serviceability demands rather than seismic ones. Although wind tunnel testing provides high-fidelity wind load data, its high cost and geometry-specific nature limit its applicability in early-stage response-based design.

Recent data-driven approaches, such as CNN–LSTM (CNNL) models[1], have demonstrated strong predictive capability for wind force time histories but often lack physical consistency in terms of spectral characteristics and spatial correlation. Physics-Informed Neural Networks (PINNs)[2] address this limitation by embedding physical constraints into the learning process. This study validates a two-stage PINN framework for wind force prediction. Part 1 focuses on force-level validation using independent wind tunnel data, while Part 2 investigates structural response equivalence through nonlinear analysis of a base-isolated building.

2 WIND TUNNEL DATASET

The dataset comprises wind tunnel experiments from two independent sources[3),4)], covering diverse building geometries to ensure model generalization. Measurements include multi-component wind force coefficients in along-wind (C_{fx}), across-wind (C_{fy}), and torsional moment (C_{mz}) directions, recorded simultaneously across multiple floors to preserve vertical correlation characteristics.

Training Set (12 buildings): Source A includes 5 buildings (H = 240–403 mm, $H/B = 6$, D/B = 1–6, 8–14 stories)[3)]. Source B contains 7 buildings (H = 200–500 mm, H/B = 1.5–5, D/B = 0.15–1, 4–10 stories)[4)].

Testing Set (1 building): An independent building (H = 400 mm, $H/B = 4$, $D/B = 1$, 8 stories) is completely excluded from training to evaluate generalization to unseen geometries[4)]. Table 1 summarizes the training and testing dataset configuration, including the geometric ratios and story numbers for each wind-tunnel source.

Table 1: Training and testing dataset configuration

Source	H (mm)	H/B	D/B	Stories
Training Set (12 buildings)				
A1	240	6	1.6	8
A2	240	6	3.2	8
A3	240	6	4.0	8
A4	240	6	6.0	8
A5	403	6	1.0	14
B1	300	5	1.0	9
B2	200	2	1.0	4
B3	300	3	1.0	6
B4	500	5	1.0	10
B5	500	4	0.67	10
B6	500	2.90	0.33	10
B7	500	1.50	0.15	10
Testing Set (1 building)				
B8	400	4	1.0	8

3 PINN METHODOLOGY

3.1 Model Architecture

The wind force prediction employs a two-stage PINN combining data-driven learning with physics-based regularization.

Stage 1: Data Model (CNNL) — A convolutional-recurrent network[1] reads historical wind velocity $\mathbf{U}_{t-w:t}$ and outputs baseline predictions: $\hat{\mathbf{C}}_{\text{base}}(t) = [\hat{C}_{fx}(t), \hat{C}_{fy}(t), \hat{C}_{mz}(t)]^T$.

Stage 2: Physics Head — A correction network outputs physics-informed adjustment: $\hat{\mathbf{C}}_{\text{PINN}}(t) = \hat{\mathbf{C}}_{\text{base}}(t) + \alpha\Delta_{\text{net}}(\hat{\mathbf{C}}_{\text{base}}(t), \mathbf{U}(t))$ where $\alpha \in [0, 0.1]$ prevents complete override of the data model. This design stabilizes training by retaining data-driven capacity while limiting the magnitude of correction to a physically plausible range.

3.2 Physics-Informed Loss Functions

The total training objective integrates data fidelity with multiple physics-based regularization terms that constrain temporal smoothness, spectral characteristics, and spatial correlation of predicted wind forces:

$$\mathscr{L} = \lambda_{\text{data}}\mathscr{L}_{\text{data}} + \lambda_{\text{rate}}\mathscr{L}_{\text{rate}} + \lambda_{\text{cov}}\mathscr{L}_{\text{cov}} + \lambda_{\text{psd}}\mathscr{L}_{\text{psd}} + \lambda_{\text{coh}}\mathscr{L}_{\text{coh}} \tag{1}$$

where $\lambda_\bullet$ denote weighting coefficients for each loss component.

(1) Data Fidelity Loss The data loss enforces agreement between predicted and measured wind force coefficients:

$$\mathscr{L}_{\text{data}} = \frac{1}{N}\sum_{k=1}^{N} \left\| \hat{\mathbf{C}}(t_k) - \mathbf{C}(t_k) \right\|_2^2 \tag{2}$$

where $\hat{\mathbf{C}}(t_k) = [\hat{C}_{fx}, \hat{C}_{fy}, \hat{C}_{mz}]^{\mathrm{T}}$ denotes the predicted force coefficient vector at time t_k, $\mathbf{C}(t_k)$ is the corresponding wind tun-

nel measurement, and N is the total number of temporal samples.

(2) Time-Rate Consistency Loss To suppress non-physical rapid oscillations, a temporal rate constraint is imposed:

$$\mathscr{L}_{\text{rate}} = \frac{1}{N-1}\sum_{k=1}^{N-1}\left\|\frac{\hat{\mathbf{C}}(t_{k+1})-\hat{\mathbf{C}}(t_k)}{\Delta t}\right\|_2^2 \tag{3}$$

where Δt is the sampling interval.

(3) Cross-Component Covariance Loss The covariance structure among force components is preserved using:

$$\mathscr{L}_{\text{cov}} = \left\|\Sigma_{\hat{\mathbf{C}}} - \Sigma_{\mathbf{C}}\right\|_F^2 \tag{4}$$

where $\Sigma_{\hat{\mathbf{C}}}$ and $\Sigma_{\mathbf{C}}$ denote the covariance matrices of predicted and reference force coefficients, respectively, and $\|\cdot\|_F$ is the Frobenius norm. This loss maintains physically consistent coupling between along-wind, across-wind, and torsional components.

(4) Power Spectral Density Loss To enforce realistic frequency-domain characteristics, the normalized power spectral density (PSD) is constrained:

$$\mathscr{L}_{\text{psd}} = \frac{1}{3}\sum_{q\in\{fx,fy,mz\}}\left\|\widetilde{S}_q^{\text{pred}}(f)-\widetilde{S}_q^{\text{ref}}(f)\right\|_2^2 \tag{5}$$

where $\widetilde{S}_q(f)$ denotes the PSD normalized by its total energy for component q, and superscripts "pred" and "ref" indicate predicted and reference spectra, respectively. This constraint preserves physically meaningful energy distribution across frequency bands.

(5) Inter-Story Coherence Loss Spatial correlation along the building height is enforced using an inter-story coherence loss:

$$\mathscr{L}_{\text{coh}} = \frac{1}{|P|}\sum_{(i,j)\in P}\left\|\hat{\gamma}_{ij}(f)-\gamma_{ij}(f)\right\|_2^2 \tag{6}$$

where $\gamma_{ij}(f)$ is the magnitude-squared coherence between stories i and j at frequency f, $\hat{\gamma}_{ij}(f)$ is the predicted coherence, and P denotes the set of considered story pairs. This loss ensures physically realistic vertical correlation of wind forces.

4 VALIDATION RESULTS

4.1 Training Performance

Figure 1 presents regression analysis of PINN-predicted versus true force coefficients. The model achieves excellent accuracy with $R^2 = 0.928$ (Cfx), $R^2 = 0.932$ (Cfy), and $R^2 = 0.817$ (Cmz). RMSE values of 0.087, 0.124, and 0.026 indicate tight clustering around ideal prediction.

Beyond point-wise accuracy, the regression slope remains close to unity for all components, indicating minimal systematic bias over the full dynamic range. Importantly, errors do not concentrate in extreme events: high-amplitude gust-driven peaks and troughs remain within the same error envelope as moderate fluctuations, which is critical for downstream response estimation where tail behavior governs demand.

Residual analysis confirms that prediction errors remain approximately symmetric without floor-dependent bias, ensuring robustness for subsequent structural response evaluation. The observed stability indicates that the proposed physics head acts as a regularizer that improves robustness without compromising overall accuracy.

4.2 Time-History Comparison (Top Floor)

Wind force time histories are inherently stochastic, and strict point-wise agreement between predicted and measured signals is neither expected nor required for engineering applications. Therefore, time-history comparison is presented only as a representative example to confirm that the predicted signals exhibit physically reasonable amplitude, intermittency, and temporal continuity.

Figure 2 shows the time-history comparison at the top floor (25F) for along-wind, across-wind, and torsional components. The PINN predictions reproduce the overall fluctuation level and intermittency observed in the reference data, without introducing spurious oscillations or artificial periodicity. This confirms that the proposed model generates temporally realistic wind force signals suitable for long-duration structural response analysis.

4.3 Height-wise Distribution of Mean and Standard Deviation

While time-history comparison is useful for confirming temporal realism, quantitative evaluation for wind-resistant design should be based on statistical measures that directly govern structural demand. In particular, the height-wise distributions of mean and fluctuating wind effects play a central role in estimating base shear, overturning moment, and story-wise response.

Figure 3 presents the height-wise distributions of the mean along-wind force and the standard deviations of along-wind force, across-wind force, and torsional moment. The mean along-wind component, which dominates quasi-static loading, is accurately reproduced over the entire building height. In addition, the predicted standard deviations show close agreement with the reference results for all components, indicating that the fluctuating wind effects are properly captured.

Compared with the baseline CNNL method, the proposed PINN significantly reduces deviations in both mean and standard deviation, particularly in the upper stories where wind-induced responses are most critical. These results demonstrate that the proposed method provides an improved representation of the statistical characteristics required for reliable response-based wind design.

4.4 Power Spectral Density Analysis

Figures 4-5 compare PSD among baseline CNNL, proposed PINN, reference, and AIJ standards. Quantitative compari-

son of variance σ^2 (PSD integral) demonstrates the superiority of physics-informed constraints. In the along-wind direction, baseline CNNL yields $\sigma^2_{\text{CNNL}} = 1{,}402{,}958$ versus reference $\sigma^2_{\text{Ref}} = 1{,}798{,}664$ (22.0% error). The proposed PINN achieves $\sigma^2_{\text{PINN}} = 1{,}897{,}265$ with only 5.5% error—a fourfold improvement. For across-wind, CNNL produces $\sigma^2_{\text{CNNL}} = 196{,}680$ (28.0% error) while PINN reaches $\sigma^2_{\text{PINN}} = 253{,}119$ (7.3% error), representing nearly fourfold accuracy gain. In torsion, PINN ($\sigma^2_{\text{PINN}} = 3{,}753{,}343$, 5.1% error) outperforms CNNL ($\sigma^2_{\text{CNNL}} = 2{,}967{,}607$, 25.0% error) with fivefold improvement.

The physics-informed constraints ensure realistic energy distribution across frequency bands. CNNL exhibits systematic energy underestimation, particularly at low frequencies governing quasi-static demand and at vortex-shedding peaks, while PINN preserves broadband characteristics consistent with reference spectra. By constraining spectral shape through physics regularization, PINN provides reliable force time histories for structural response prediction where energy accuracy directly impacts design demand estimation.

4.5 Inter-Story Coherence Analysis

Figures 6–8 present the vertical coherence of wind forces between floors. The proposed coherence constraint reproduces the physically expected decay with story separation for along-wind components and preserves organized correlation near characteristic frequencies such as vortex shedding. As a result, the predicted loading maintains realistic spatial correlation across floors, which is essential for accurate modal superposition and response estimation in base-isolated buildings.

4.6 Generalization and Robustness on Unseen Geometry

A key objective is to verify that the proposed method generalizes beyond the training set. The held-out building provides an unseen geometry with distinct aerodynamic characteristics. Despite exclusion from training, the PINN maintains consistent accuracy and physics consistency across all three components. In particular, PSD and coherence agreement remain stable, indicating that the embedded physical constraints guide extrapolation toward physically plausible signals even under new geometric conditions.

This behavior contrasts with purely data-driven models, which may fit training geometries well but degrade on unseen shapes due to shortcut learning. The proposed two-stage architecture mitigates this risk: the baseline model captures generic temporal structure, while the physics head corrects deviations that would violate spectral and coherence constraints, leading to improved robustness for design applications.

5 CONCLUSIONS

This study validated a two-stage physics-informed neural network for wind load prediction using independent wind tunnel data and AIJ-consistent physical constraints. The proposed method achieves high predictive accuracy while preserving realistic temporal behavior, spectral characteristics, and inter-story coherence required for structural response estimation. Part 2 will further quantify the impact on base-isolated structural responses.

REFERENCES

1. Bao Y, Pei C, Mou Y, Li M, Cheng X. A convolutional neural network–long short-term memory (CNN–LSTM)–Attention model based on wavelet transform for predicting non-stationary wind pressure coefficients on the surface of terminal glass curtain wall. Science Progress. 2025;108(3).
2. Raissi, M., et al.: Physics-informed neural networks, *J. Comput. Phys.*, 378, 686-707, 2019.
3. Hiratsuka, K., et al.: Elasto-plastic wind-induced response evaluation of a passively controlled high-rise building with hysteretic damper, *AIJ J. Technol. Des.*, 27(66), 662-667, 2021.
4. Hirai, H., et al.: Influence of numbers of experimental wind force samples on wind response analysis of a tall building, *AIJ J. Technol. Des.*, 18(39), 489-494, 2012.
5. Eivazi, H., et al.: PINNs for solving RANS equations, *Phys. Fluids*, 34(7), 075117, 2022.
6. Li, S., et al.: Frequency-domain PINN for 3D wind fields, *Appl. Energy*, 382, 126256, 2025.
7. AIJ: Recommendations for Loads on Buildings, Ch. 6: Wind Loads, 2015.

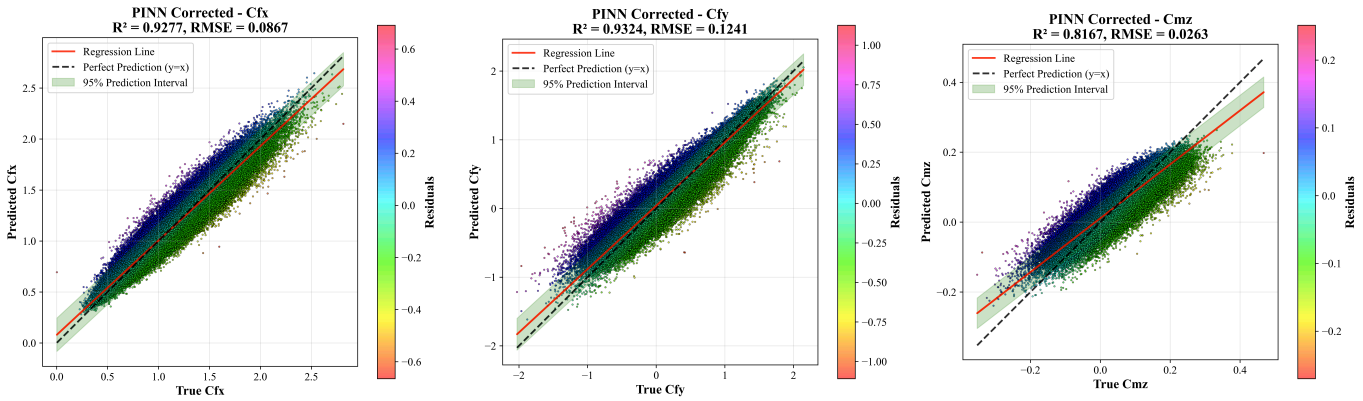

Figure 1: Regression analysis of PINN predictions: Cfx (left), Cfy (middle), Cmz (right)

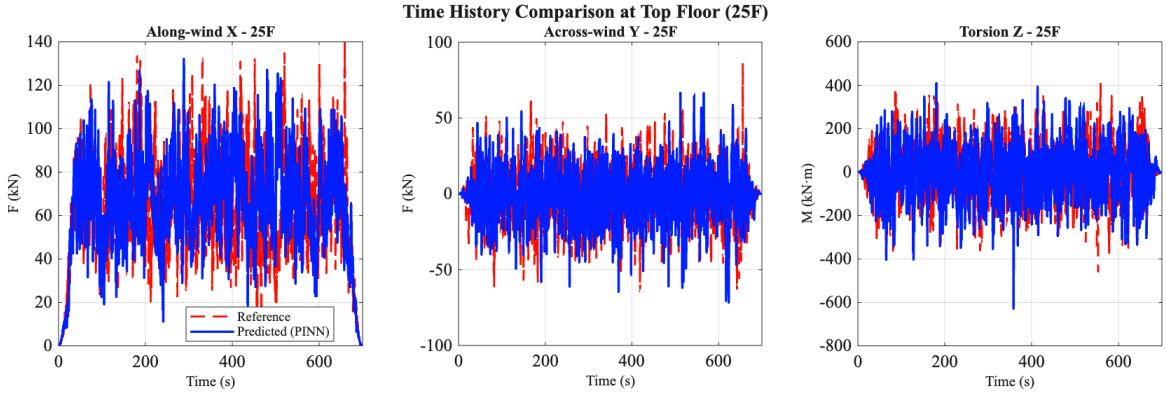

Figure 2: Representative time-history comparison at the top floor (25F): along-wind (X), across-wind (Y), and torsion (Z)

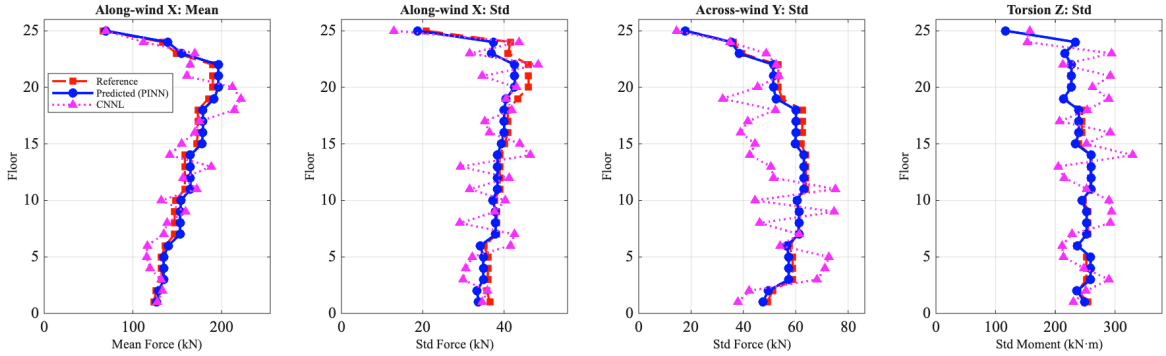

Figure 3: Height-wise distributions of mean and standard deviation of wind effects: comparison among PINN prediction, reference, and baseline CNNL method

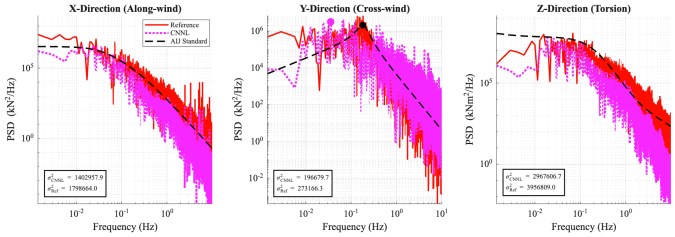

Figure 4: Baseline CNNL PSD vs AIJ

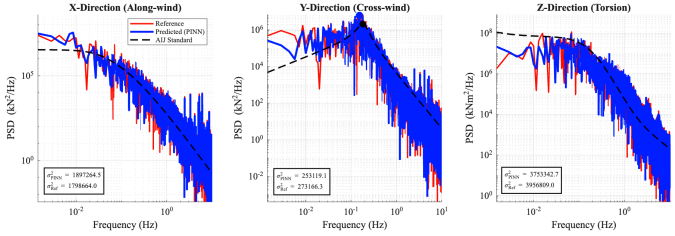

Figure 5: PINN PSD: Predicted, Reference, AIJ

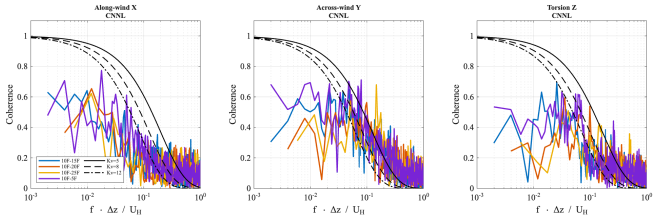

Figure 6: Baseline CNNL coherence

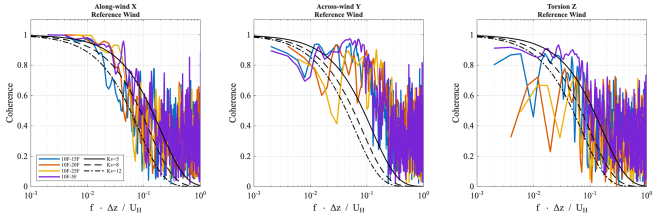

Figure 7: Reference wind force coherence

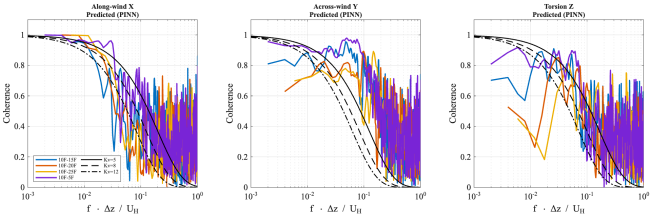

Figure 8: PINN predicted coherence functions

*1　東京科学大学　大学院生
*2　東京科学大学　総合研究院　准教授・博士(工学)
*3　東京科学大学　総合研究院　助教・博士(学術)
*4　株式会社竹中工務店　技術研究所

Graduated Student, Institute of Science Tokyo*1
Associate Prof., IIR, Institute of Science Tokyo, Dr.Eng.*2
Assistant Prof., IIR, Institute of Science Tokyo, Ph.D.*3
Research & Development Institute, Takenaka Corporation*4